Probe spectroscopy in an operating magneto-optical trap: The role of Raman transitions between discrete and continuum atomic states

Tomasz M. Brzozowski,* Maria Brzozowska, Jerzy Zachorowski, Michał Zawada, and Wojciech Gawlik
Marian Smoluchowski Institute of Physics, Jagiellonian University, Reymonta 4, PL 30-059 Cracow, Poland†
(Received 18 August 2004; published 3 January 2005)

We report on cw measurements of probe beam absorption and four-wave-mixing spectra in a ^{85}Rb magneto-optical trap taken while the trap is in operation. The trapping beams are used as pump light. We concentrate on the central feature of the spectra at small pump-probe detuning and attribute its narrow resonant structures to the superposition of Raman transitions between light-shifted sublevels of the ground atomic state and to atomic recoil processes. These two contributions have different dependencies on trap parameters and we show that the former is inhomogeneously broadened. The strong dependence of the spectra on the probe-beam polarization indicates the existence of large optical anisotropy of the cold-atom sample, which is attributed to the recoil effects. We point out that the recoil-induced resonances can be isolated from other contributions, making pump-probe spectroscopy a highly sensitive diagnostic tool for atoms in a working magneto-optical trap.

DOI: 10.1103/PhysRevA.71.013401 PACS number(s): 32.80.Pj, 42.50.Vk, 42.65.−k

I. INTRODUCTION

The magneto-optical trap (MOT) is now a standard tool for obtaining cold atomic samples. Due to significantly reduced Doppler broadening, low collision rate, and long interaction time, such samples offer a unique possibility of ultraprecise spectroscopic measurements. They are especially useful for experiments which investigate Raman transitions between nearly degenerate energy levels. The resonant structures in probe spectra observed in cold media for pump-probe detuning much smaller than the natural linewidth are due to numerous effects: stimulated Rayleigh scattering [1] and Raman transitions between either light shifted sublevels of a ground atomic state [2], vibrational energy levels of atoms localized in an optical lattice [3], or kinetic momentum states of unbound atoms [4]. However, the MOT is not an ideal tool for systematic investigation of these effects. Because of the fixed three-dimensional geometry of the trapping beams, the presence of inhomogeneous trapping magnetic field, and limited flexibility in varying the trap parameters, it is difficult to selectively address the phenomena mentioned above. This is why the MOT usually serves only as an initial stage of preparation of a cold sample which, after switching off the MOT's optical and magnetic fields, is subject to more precisely controlled experimental conditions, such as dedicated pump beam geometry and polarization [1,4–7], phase-stabilized pump beams [8], etc.

Despite these difficulties, cw pump-probe spectroscopy of trapped atoms performed while the MOT is working, using the trapping beams as pump light, has been studied by several authors. Such experiments were carried out by Tabosa *et al.* [9] and Grison *et al.* [2]. Also, there exists spectroscopic evidence of optical lattices in a MOT with a special, phase-shift-insensitive, trapping beam geometry [10]. These experiments indicated the potential of probe spectroscopy for cold-atom diagnostics. However, the complexity of such spectra from a working MOT resulted in their possible application for MOT diagnostics being neglected. In this paper we revisit the problem and describe our systematic studies of such spectra.

The aim of this paper is to examine the Raman processes which occur in a MOT. Their interplay makes the MOT spectra far more complex than those obtained under simpler experimental conditions. The systematic study of the MOT spectra is necessary for their possible application for MOT diagnostics which, as we show below, can be successfully performed by pump-probe spectroscopy. Working MOT spectroscopy can constitute a powerful, nondestructive diagnostic tool. It can provide information on the atomic cloud density [11] and average Rabi frequency [12]. Below, we concentrate on the additional possibility of spectroscopic velocimetry of atoms in a working MOT, based on the recoil-induced resonances (RIR). This method has been already successfully used to determine the temperature of the cold sample [4,13–15] but under conditions in which RIR constituted the only relevant contribution to the spectra. In a working MOT, however, recoil-induced resonances appear accompanied by the other Raman processes which necessitates clear identification and more thorough analysis of their individual contributions.

Below, in Sec. II, we briefly characterize our setup and in Sec. III present in more detail our experiment and results. We perform spectroscopic measurements of ^{85}Rb atoms in a standard MOT [16]. With the MOT's optical and magnetic fields still turned on, we simultaneously record two signals: a probe absorption and a four-wave mixing signal. The latter is generated by atoms as a result of their nonlinear interaction with the probe and trapping beams and in such a geometry propagates oppositely to the probe beam direction [17]. The spectroscopic signals were acquired for various trap parameters, e.g., the trapping beams' intensity and detuning from atomic resonance and the gradient of the MOT's magnetic field. This allowed us to carry out a systematic investigation of the phenomena that affect the shapes of the absorption and four-wave mixing spectra.

*Electronic address: tmb@ceti.pl
†URL: http://www.if.uj.edu.pl/ZF/qnog/

In Sec. IV, we show that the theoretical explanation of the observed spectra has to include two contributions: the Raman resonances between light-shifted Zeeman sublevels of the ^{85}Rb $^2S_{1/2}$ ($F=3$) ground state, or for short, the Raman-Zeeman resonances (RZR's) [2,18] and the recoil-induced resonances (RIR's) [4,19,20]. Additionally, in order to reach good agreement between the theory and the experimental data, one has to consider realistic physical conditions in the MOT, namely, the light intensity and polarization gradients, the three-dimensional geometry of the trapping beams, and the inhomogeneity of the quadrupole MOT's magnetic field. In Sec. IV we present interpretation of the main individual mechanisms that can be recognized in the MOT. We also note that the difference between the σ^+ and σ^- absorption spectra is the signature of the optical anisotropy of the cold atomic sample in a MOT and is due to recoil resonances induced by the probe and different trapping beams. Finally, we suggest a method to eliminate the RZR contribution, thus opening the possibility of real-time, nondestructive MOT temperature measurement based on observation of the width of RIR contribution [4], and we conclude our work in Sec. V.

II. EXPERIMENTAL SETUP

We use a standard magneto-optical trap [21] in a stainless-steel vacuum chamber with antireflection coated windows. Our laser setup consists of four home-built diode lasers. One of them, equipped with an external cavity, is frequency stabilized using saturated absorption in a rubidium vapor cell, or alternatively the Doppler-free dichroism method [22]. This laser serves as the master for injection seeding into the trapping and probe lasers. The 780-nm light from a 70-mW trapping diode laser is divided into three beams, which have Gaussian radius $\sigma \approx 0.4$ cm and peak intensity $I_{\max} = 12$ mW/cm^2. They are retroreflected after passing the trap cell. The frequency shift of the trapping and probe beams is controlled by several acousto-optic modulators (AOM's). The typical detuning, $\Delta = \omega - \omega_0$, of the trapping beams of frequency ω from the trapping transition resonance frequency ω_0 is -3Γ, where $\Gamma = 2\pi \times 5.98$ MHz is the transition's natural linewidth. Before injection into the probe laser diode, the master beam double passes the AOM, which allows us to tune the frequency $\omega_{\rm pr}$ of the probe laser in the range of ±40 MHz around the master laser frequency. In the present experiment the probe sweep range was ±3 MHz. Since both trapping and probe lasers are seeded with the same beam, they are phase locked. Thus when these two lasers work in the pump-probe configuration they provide a spectroscopic resolution which allows one to distinguish resonant structures with widths of a few kHz, limited by residual phase fluctuations. The repumping beam is derived from an independent, free running laser diode, and is overlapped with one of the trapping beams. The quadrupole magnetic field is generated by a pair of anti-Helmholtz coils, which produce an axial gradient of 16 G/cm. Stray dc magnetic fields are zeroed by three orthogonal pairs of Helmholtz coils. We trap about 10^7 atoms in the cloud with a Gaussian radius of $\sigma \approx 0.9$ mm. The temperature of our sample, measured by the time-of-flight method [23], is about 100 μK.

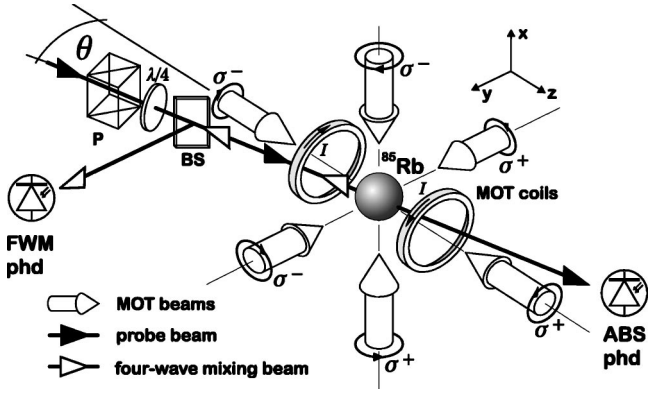

FIG. 1. The geometry of the experimental setup.

The geometry of our experiment is depicted in Fig. 1. The probe beam enters the cloud of cold atoms at a small angle $\theta = 3.5°$ with one of the trapping beams. The polarization of the probe beam is set by the $\lambda/4$ waveplate placed after a polarizer (P). We define the polarization of the probe beam with respect to the nearly co-propagating trapping beam, which is σ^- polarized. We call the probe polarization σ^- (σ^+) when it is the same as that of the nearly co-propagating (counterpropagating) trapping beam. After traversing the cloud, the probe beam is directed onto a photodiode which records the absorption spectrum (ABS phd). The four-wave mixing beam, generated in the cloud and propagating oppositely to the probe beam, is reflected by a 50/50 beamsplitter (BS) onto another photodiode (FWM phd). Both signals are acquired simultaneously and thus can be directly compared. The probe beam is shaped to have the diameter smaller than the cloud size in order to avoid an undesired background of nonabsorbed light. Typically, the probe-laser power is about 1 μW, and its frequency is swept at a rate of 5 MHz/s. The spectra presented in this paper are recorded as a function of the pump-probe detuning, $\delta = \omega_{\rm pr} - \omega$, and are averaged over 20 probe sweeps.

III. MEASUREMENTS AND RESULTS

We have performed systematic studies of absorption and four-wave mixing spectra of ^{85}Rb atoms in a MOT. We have varied the trapping beams' intensity, their detuning, and the magnetic-field gradient. Examples of absorption and four-wave-mixing spectra simultaneously recorded for three various trapping beam intensities are depicted in Fig. 2. The shapes of the spectra are similar to those previously observed and assigned to RZR (see, for example, Refs. [2,9]). However, in contrast to the pure RZR case, they differ significantly for σ^+ (left column) and σ^- polarization of the probe beam (right column). In particular, in absorption, the σ^+ and σ^- spectra have different amplitudes and positions of individual resonances. In four-wave mixing, the spectra consist of two very distinct contributions, one broad and second ultranarrow. The broad contribution to the wave-mixing spectra recorded with the σ^+ probe appears broader that that associated with the σ^- probe.

From Fig. 2 it is clearly seen that with the increase of the trapping beam intensity, both the absorption and four-wave-

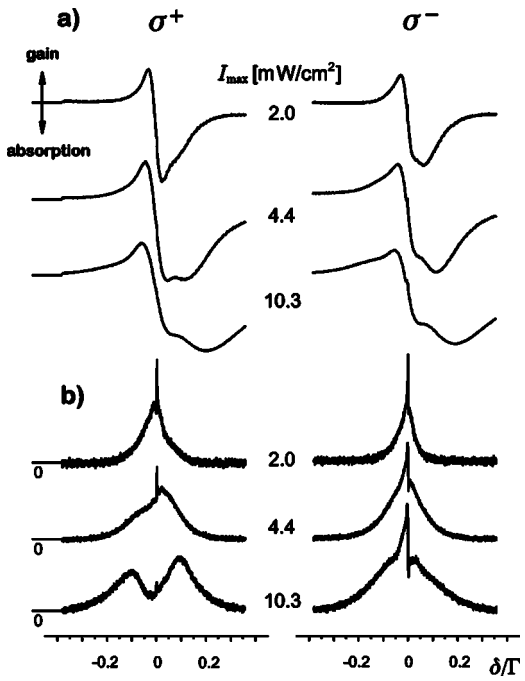

FIG. 2. Probe absorption spectra (a) and four-wave mixing signals (b) for the σ^+ and σ^--polarized probe beam. The spectra are recorded as a function of the pump-probe detuning δ. I_{max} stands for the peak intensity of a single trapping beam. The trapping beam detuning from atomic resonance is $\Delta=-3\Gamma$, the magnetic field gradient along coil axis is $\partial B/\partial z=13$ G/cm.

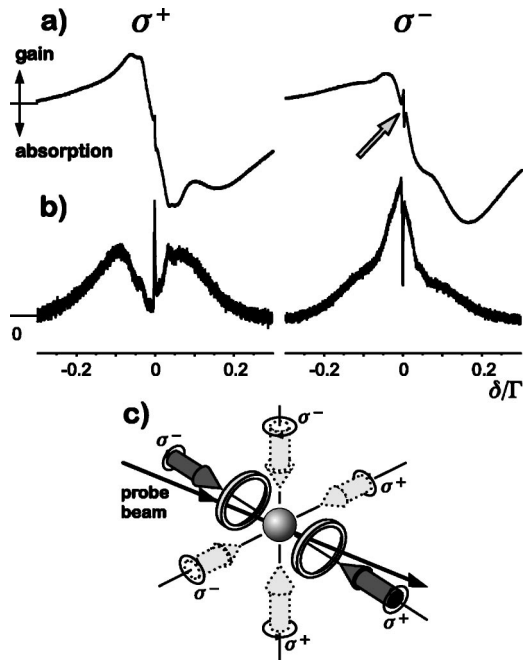

FIG. 3. Probe absorption spectra (a) and four-wave mixing signal (b), recorded when almost all trapping beam power is sent to the pair of trapping beams nearly collinear with the probe, as schematically shown in (c). The intensity of these beams is $I_z=30$ mW/cm^2, intensity of beams transversal to the probe beam is 3 mW/cm^2. The detuning of the trapping beams is $\Delta=-3\Gamma$ and the magnetic-field gradient is $\partial B/\partial z=13$ G/cm. The dispersive shape of the recoil-induced resonance shows up in the center of the σ^--polarized probe absorption spectrum (marked by gray arrow).

mixing spectra become wider and their resonant structures better resolved. This fact can be qualitatively explained by the increase of the splitting of the ground-state Zeeman sublevels due to the ac Stark shift (light shift). For $\Omega>\Gamma$, this shift is proportional to the pump beam intensity (Ω is the Rabi frequency associated with the pump field). The quantitative description of the shape of the spectra, however, should incorporate all possible Raman transitions between the pairs of adjacent Zeeman sublevels in the $^2S_{1/2}$ $(F=3)$ ground state of ^{85}Rb [see Fig. 4(a) below] and also include a possible RIR contribution. This will be discussed in the next section.

In the case of the absorption spectra for the σ^--polarized probe, a weak, ultranarrow structure appears near the pump-probe detuning $\delta\approx 0$. In the four-wave mixing signal this ultranarrow resonance is even more pronounced and occurs for both polarizations of the probe beam. This feature in a MOT spectra has not yet been thoroughly examined. We attribute it to recoil-induced resonances [4]. To verify this hypothesis we have performed an additional measurement. The trapping beam intensities were set in such a way that almost all trapping laser power was sent to the pair of trapping beams nearly collinear with the probe. In such a situation, trapping beams transverse to the probe are much attenuated and serve only to sustain the cloud stability. Thus we approach the one-dimensional pump-probe spectroscopy setup with two counterpropagating strong pump beams nearly collinear with the probe [5], while still having cold atomic cloud in a stable MOT. Spectra registered under such conditions, presented in Fig. 3, reveal resonant structures around $\delta\approx 0$ even better resolved than those of Fig. 2. In particular, a distinct dispersionlike resonance develops in the center of the absorption spectrum for the σ^--polarized probe, while for the σ^+ probe polarization it is barely visible. The shape of this resonance agrees well with the theory of recoil-induced resonances [4] and its width corresponds to the actual temperature of the atomic sample, which has been measured independently [23].

In order to understand how the measured spectra depend on realistic MOT conditions we have measured the absorption and four-wave mixing spectra for various magnetic-field gradients. Since the size of the cloud is proportional to $(\partial B/\partial z)^{-1/2}$ [16], the value of the magnetic field in the peripheries of the cloud scales as $(\partial B/\partial z)^{1/2}$. For a well-aligned MOT with the value $B=0$ in the trap center, we observed that for smaller gradients the resonances occur at the same frequencies as for larger gradients but are better resolved. Thus due to the finite size of the atomic cloud, when modeling the experimental curves one has to take into account the inhomogeneous broadening due to the MOT quadrupole magnetic field.

IV. INTERPRETATION

The shape of the absorption and four-wave mixing spectra that we measure in our experiment can be explained on the basis of two processes: Raman transitions between light-

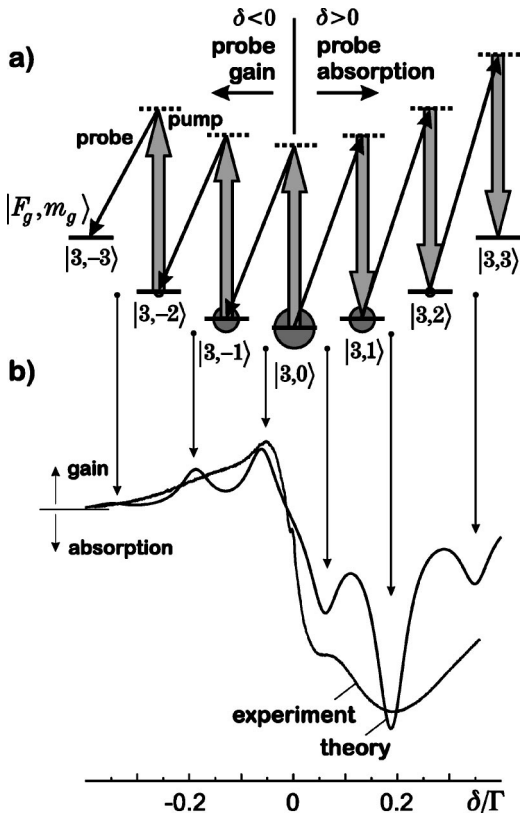

FIG. 4. (a) Multilevel structure of the $5\,^2S_{1/2}\,(F=3)$ ^{85}Rb ground state. Zeeman sublevels are perturbed with a π-polarized pump (thick gray arrows), which results in their energy shift and symmetric population distribution (alignment), marked by gray circles. The structure is then probed by a σ^+-polarized beam. (b) Theoretical absorption signal compared with the experimental spectrum. The theoretical curve was generated for the Rabi frequency $\Omega=6\Gamma$, detuning $\Delta=-3\Gamma$ and $\gamma_{i,k}=0.13\Gamma$ for all i,k. Experimental conditions: $I_{\max}=10.2\ \mathrm{mW/cm^2}$, $\Delta=-3\Gamma$, $\partial B/\partial z=13\ \mathrm{G/cm}$.

shifted Zeeman sublevels (RZR) of the ground state [2,24] and recoil-induced resonances (RIR) [4]. The theoretical outline of both processes is presented below. However, in order to perform the complete modeling of the spectra, we extended the present theories by inclusion of two types of inhomogeneous broadening: one due to modulation of the net **E** field in the trap and the other connected with the presence of the quadrupole trapping magnetic field **B**. Moreover, the standard three-dimensional geometry of the MOT beams has to be taken into account when considering recoil processes in a working trap.

A. Raman transitions between light-shifted Zeeman sublevels (RZR)

Let us consider the cycling $5\,^2S_{1/2}\,(F_g=3)-5\,^2P_{3/2}\,(F_e=4)$ transition in ^{85}Rb atom in a MOT. The atom is subject to three pairs of counterpropagating laser beams of frequency ω with pairwise orthogonal circular polarizations. Their interference in the intersection region results in a complex spatial modulation of light intensity and polarization [25]. For the sake of simplicity, we consider here only the case where the net light field is linearly polarized and choose quantization axis parallel to the local direction of the net field **E**. In this reference frame, the resulting pump light is π polarized and shifts the Zeeman sublevels of both the ground and the excited atomic state. The $5\,^2S_{1/2}\,(F_g=3)$ ground state multilevel structure is presented in Fig. 4(a). The optical pumping in such a scheme leads to alignment, i.e., a symmetric distribution of populations with respect to the $m_g=0$ sublevel of the ground state, with this sublevel being mostly populated. The atoms interacting with the pump light are probed by circularly polarized weak probe laser [26]. The Raman processes involving a π-polarized pump and a $\sigma^{\pm}$-polarized probe photon lead to transitions with $\Delta m_g=\pm 1$. For a given population distribution among the m_g sublevels, two directions of such processes are possible, depending on the sign of the probe-pump detuning δ. In the considered case of dominant population in the $m_g=0$ sublevel, the Raman transitions with $\Delta m=-1$ take place for $\delta<0$ and lead to gain of the probe; those with $\Delta m=+1$ take place for $\delta>0$ and result in its attenuation. These processes are resonant whenever $|\delta|$ coincides with the energy separation of the adjacent sublevels. The amplitude of the corresponding resonance is proportional to the population difference of the sublevels involved in the transition and depends on the Clebsch-Gordan coefficients associated with the specific transition path. The simplest model of the probe absorption spectrum is obtained by summing the Lorentzian profiles centered at the appropriate resonance frequencies and weighted by products of the relevant population differences and squares of the Clebsch-Gordan coefficients,

$$s_{\mathrm{RZR}}(\delta)=\sum_{i=1}^{3} w_{i-1,i}\Delta\Pi_{i-1,i}L(\delta,\delta_{i-1,i},\gamma_{i-1,i}) - \sum_{i=-1}^{-3} w_{i+1,i}\Delta\Pi_{i+1,i}L(\delta,\delta_{i+1,i},\gamma_{i+1,i}). \qquad (1)$$

In the above equation, $w_{k,j}$ is the weight associated with the Clebsch-Gordan coefficient along the $k=m_g\leftrightarrow j=m_g$ Raman transition path, $\Delta\Pi_{k,j}$ is the population difference of the $k=m_g$ and $j=m_g$ sublevels, and the Lorentzian profile is given by

$$L(\delta,\delta_{k,j},\gamma_{k,j})=\frac{\gamma_{k,j}}{\gamma_{k,j}^2+(\delta-\delta_{k,j})^2}, \qquad (2)$$

where $\delta_{k,j}$ and $\gamma_{k,j}$ are, respectively, the resonance frequencies and widths of the $k=m_g\leftrightarrow j=m_g$ transitions. These widths are due to the optical pumping, the finite interaction time, and atomic collisions in a trap. The spectrum generated using formula (1) with assumption of full optical pumping in the closed system shown in Fig. 4(a) is presented in Fig. 4(b) compared to the relevant experimental data. The comparison shows that the latter constitutes an envelope for the theoretical curve under which individual resonances are unrealistically well resolved. This suggests a broadening mechanism, which is indeed provided by the spatial inhomogeneity of the light intensity in the trap. To account for this effect, we averaged the calculated spectra over Rabi frequency Ω. This can be done as described in Ref. [27], but in our case it was

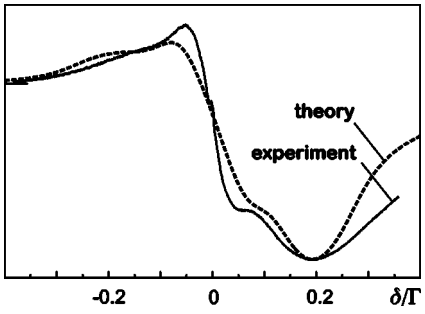

FIG. 5. The comparison of experimental absorption spectrum [acquired under the same experimental conditions as in Fig. 4(b)] with the theoretical curve generated according to Eq. (1) and averaged over the Rabi frequency range $\Omega \in [5\Gamma; 7.5\Gamma]$.

sufficient to sum the absorption spectra generated according to Eq. (1) for the appropriate range of Rabi frequencies. By numerical simulations of various field contributions, similar to that of Ref. [25], we have found that the relevant range that produces the best agreement between the theory and the experiment is $5\Gamma - 7.5\Gamma$. This corresponds to the average Rabi frequency of 6.25Γ determined as in Ref. [12]. The inclusion of the **E**-field inhomogeneity yields a better agreement of theoretical results with the experimental data, as presented in Fig. 5. However, there is still a discrepancy between the theoretical prediction and the experimental signal near $\delta \approx 0$. Moreover, the model discussed above does not explain the profound difference between the spectra registered for σ^+ and σ^--polarized probe. The explanation of this effect is presented in the next subsection.

B. Recoil-induced resonances (RIR)

The momentum exchange between nonlocalized atoms and the laser field is associated with the phenomenon of the so-called recoil-induced resonances (RIR). They were predicted by Guo *et al.* [20] and observed by Grynberg *et al.* [4,5]. A simple momentum-space analysis of RIR can be found in Refs. [4,15,19]. Here we briefly recall its results.

Let us consider atoms of mass m interacting with a weak probe beam (with wave vector $\mathbf{k}_{\rm pr}$ and frequency $\omega + \delta$), which makes an angle θ with the direction of propagation of a strong pump beam (wave vector $\mathbf{k}$, frequency ω), as depicted in Fig. 6(a). The process of pump photon absorption followed by the probe photon emission results in the momentum change Δp of an atom, where

$$\Delta p = -2\hbar k \sin\frac{\theta}{2}. \tag{3}$$

The preceding equation is derived assuming small probe-pump detuning $|\mathbf{k}| \approx |\mathbf{k}_{\rm pr}| = k$. The resonance occurs whenever the probe-pump detuning coincides with the kinetic energy difference, namely at detuning

$$\delta_{\rm res} = -\frac{2k}{m}\left(\hbar k \sin\frac{\theta}{2} - p\right)\sin\frac{\theta}{2}. \tag{4}$$

An analogous consideration performed for the case of probe-photon absorption followed by emission of a photon into the

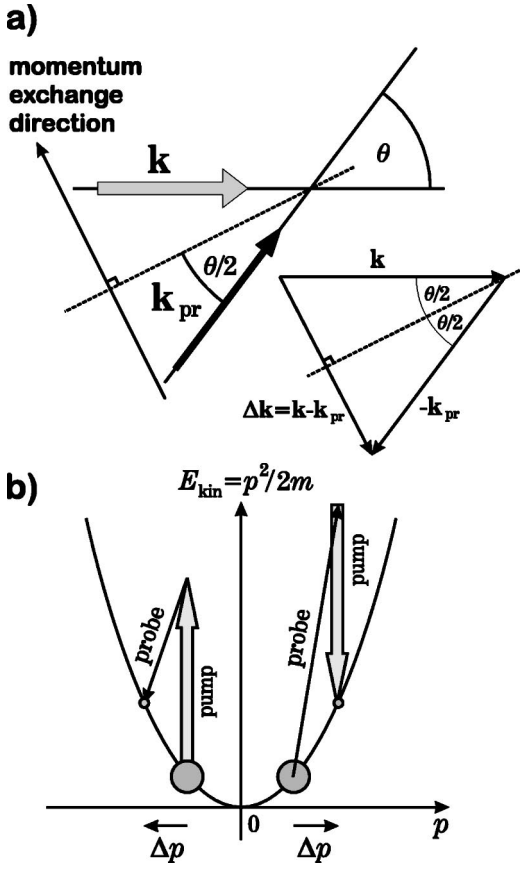

FIG. 6. (a) Basic geometry for the recoil induced resonance, associated with atomic interaction with two beams: the pump (thick gray arrow) and probe (thin arrow) beams intersecting in an atomic sample at a small angle θ. (b) Raman transitions between the kinetic momentum states for an atom in a state with specific m_g.

pump beam leads to the nearly identical formula for $\delta_{\rm res}$ as Eq. (4), but with the opposite sign. Similarly to the RZR case, the resonance amplitude is proportional to the population difference between the relevant atomic states, but now we consider the continuum, kinetic momentum states rather than discrete, magnetic sublevels [Fig. 6(b)]

$$\Delta\Pi(p_{\rm final}, p_{\rm initial}) = \Pi(p + \Delta p) - \Pi(p). \tag{5}$$

Integration over all possible momentum values leads to the formula for the RIR signal given as

$$s_{\rm RIR}(\delta, \theta) = -\int_{-\infty}^{\infty} dp \Delta\Pi(p_{\rm final}, p_{\rm initial}) L(\delta). \tag{6}$$

Assuming that $\Pi(p)$ is a Gaussian distribution, $\Delta p \ll p_T = \sqrt{m k_B T}$ and $\gamma \ll k p_T / m$ [4] (all these conditions are fulfilled in our case), one arrives at an analytic formula for the absorption spectrum signal,

$$s_{\mathrm{RIR}}(\delta,\theta) = -\sqrt{\frac{m}{2\pi}}\frac{\hbar\delta}{2u_T^{3/2}k\,\sin(\theta/2)} \times\exp\left[-\frac{\delta^2}{2u_T^2[2k\,\sin(\theta/2)]^2}\right], \tag{7}$$

where $u_T = p_T/m$ is the most probable atomic speed. The signal (7) is the derivative of a Gaussian function. It has its minimum/maximum for $\delta = \pm 2u_T k \sin(\theta/2)$ and the width of the spectrum Δ_{RIR}, defined as the distance between minimum and maximum, is proportional to $\sqrt{T}$. The RIR spectrum can thus serve as a spectroscopic tool for the temperature measurement of a cold atomic sample [4,13,14], according to the formula

$$T = \frac{m}{16k_B k^2 \sin^2(\theta/2)}\Delta_{RIR}^2. \tag{8}$$

The results presented above refer to a two-level atom and a simple pump-probe beam configuration. Nevertheless, this simple approach can be also successfully used in our case in which multilevel atoms are subject to a three-dimensional set of trapping beams. Since a distinct RIR contribution appears only near $\delta \approx 0$ (see Figs. 2 and 3), it must result from Raman transitions between the momentum states of the same magnetic sublevel, $\Delta m_g = 0$. In principle, RIR's can also occur between momentum states associated with various Zeeman sublevels, i.e., with $\Delta m_g \neq 0$, in which case some σ^+/σ^- asymmetry might be visible, but this contribution to the overall signal is negligible. First, the amplitudes of such contributions have been shown to be about order of magnitude weaker than of the $\Delta m_g = 0$ principal ones [28]. Second, they would result only in a small frequency shift of the broader RZR contribution. Third, as shown below in Sec. IV C, the Raman transitions with $\Delta m_g \neq 0$ in a working MOT are subject to inhomogeneous broadening which further reduces their importance for RIR. Thus the recoil contribution is due to the probe and pump beams of the same polarization. This implies that our atoms can be effectively treated as two level systems [11,29] and that the polarization of the probe selects the pump of the appropriate polarization among all six available beams.

For example, consider the case in which the probe beam is σ^- polarized and the quantization axis is parallel to its direction of propagation. Obviously, one contribution to the recoil process is due to the probe beam combined with the nearly co-propagating trapping beam. Analogously, the σ^+-polarized probe interacts with the nearly counterpropagating trapping beam. The second contribution is due to the trapping beams transverse to the probe. In the chosen reference frame, these beams appear as linearly σ and π polarized. Depending on their relative phases, they represent σ^+ or σ^--polarized pump photons with the same probability, so they equally contribute to the recoil processes both for the σ^+ and σ^--polarized probe. This consideration yields the total RIR signal in the probe beam absorption in the MOT with all six trap beams as equal to

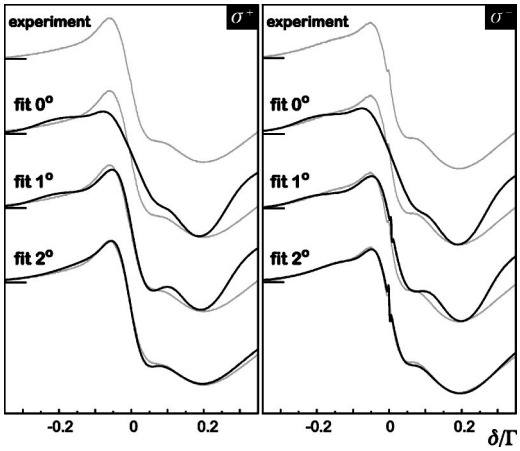

FIG. 7. Experimental and theoretical absorption spectra for σ^+ and σ^--polarized probe beam. The experimental conditions: $I_{\max} = 10.2\ \mathrm{mW/cm^2}$, $\Delta = -3\Gamma$, $\partial B/\partial z = 13\ \mathrm{G/cm}$. Fit 0° includes only inhomogeneity of the **E** field, fit 1° − as fit 0° + RIR, fit 2° − as fit 1° + inhomogeneity of the **B** field. Parameters of theoretical simulations: Rabi frequency averaging range $\Omega \in [5\Gamma; 7.5\Gamma]$; Gaussian width of a single, inhomogeneously broadened resonance $\sigma_B = 0.088\Gamma$, which corresponds to the actual trap size $\sigma_z = 0.9$ mm; the temperature of atomic cloud $T = 155\ \mu$K was fitted to achieve the best agreement of the simulation with experimental data and is consistent with the results of Ref. [23]. For better comparison, the experimental spectra are added in grey to each fit.

$$s_{\mathrm{RIR,MOT}}(\delta) = \begin{cases} s_{\mathrm{RIR}}(\delta,\theta) + 2s_{\mathrm{RIR}}(\delta,90^\circ) \\ \quad \text{for } \sigma^- - \text{polarized probe;} \\ s_{\mathrm{RIR}}(\delta,180^\circ-\theta) + 2s_{\mathrm{RIR}}(\delta,90^\circ) \\ \quad \text{for } \sigma^+ - \text{polarized probe.} \end{cases} \tag{9}$$

The above discussion allows one to associate the observed distinct difference between the MOT spectra taken for σ^- and σ^+-polarized probe exclusively with the recoil processes, since, as it was pointed out in Sec. IV A, the RZR contributions are insensitive to the probe beam polarization.

C. Influence of the MOT magnetic field

The considerations presented above lead to the conclusion that both RZR and RIR contribute to the observed spectra, so the complete formula for the absorption signal becomes

$$s(\delta) = \overline{s_{\mathrm{RZR}}}(\delta) + s_{\mathrm{RIR,MOT}}(\delta), \tag{10}$$

where $\overline{s_{\mathrm{RZR}}}(\delta)$ is the RZR contribution averaged over Rabi frequencies available in a MOT, as discussed in Sec. IV A. The results of theoretical simulations according to formula (10) are depicted in Fig. 7 (fit 1°) and compared with experimental data. While the agreement of the modeled and experimental spectra improved considerably after considering both contributions to $s(\delta)$, the theoretical spectrum still exhibits resonances that are too narrow. Simplistic attempts to reduce resolution of the theoretical spectra by extending the Ω inhomogeneity range in the $\overline{s_{\mathrm{RZR}}}(\delta)$ contribution does not improve the fit. Whereas the net spectrum $s(\delta)$ becomes broader, its individual peaks and dips are shifted out of co-

incidence with the experimental ones. This indicates that some other kind of inhomogeneous broadening mechanism must affect the spectra. This mechanism is due to the quadrupole MOT magnetic field **B** and finite size of the atomic cloud. As the spatial distribution of atomic density in the trap is Gaussian, modeling of the individual RZR resonances, such as in Eq. (1), should be performed with the Gaussian profiles $G(\delta,\delta_{k,j},B)$, rather than with the Lorentz functions (2). We thus take

$$G(\delta,\delta_{k,j},B)=C\exp\left[-\frac{(\delta-\delta_{k,j})^2}{2\sigma_B^2}\right], \tag{11}$$

with

$$\sigma_B=\frac{g_F\mu_B}{\hbar}\frac{\partial B}{\partial z}\sigma_z \gg \gamma_{k,j}. \tag{12}$$

In the above formulas, C is a constant, g_F is the Lande factor of the $^2S_{1/2}(F=3)$ hyperfine state, μ_B is the Bohr magneton and σ_z is the Gaussian radius of the atomic cloud along the z axis. The results of the theoretical simulation of the absorption spectra with inclusion of the MOT magnetic field are presented in Fig. 7 as fit 2° and are compared with the experimental data. In contrast to averaging exclusively over $|\mathbf{E}|$ (fits 0° and 1°), the agreement of the theoretical and experimental absorption signals is now very good. This indicates the importance of the inhomogeneous broadening of the MOT spectra. So far, the RZR's in a MOT have been considered to be free of any inhomogeneous broadening. Our experiment shows that this is not the case. While Doppler broadening is negligible, the magnetic-field inhomogeneities cause substantial broadening of the pump-probe Raman spectra and corresponding change of their line shapes from Lorentzian to Gaussian.

D. Four-wave mixing signals

In our experiment, the four-wave mixing spectra are recorded simultaneously with the probe beam absorption, which assures that they are acquired in exactly the same experimental conditions. The four-wave mixing signals recorded in our experiment [Figs. 2(b) and 3(b)] clearly exhibit two contributions: the broad pedestal and pronounced, ultranarrow features for $\delta\approx 0$. The former can be attributed to the superposition of the RZR's and RIR's and the latter is due to the transitions between kinetic momentum states, RIR and possibly to the Rayleigh scattering [1]. Ultranarrow resonances are here far better resolved than in the case of corresponding absorption signals. Hence the four-wave mixing spectroscopy appears to be more sensitive to the recoil effects. However, precise verification of this conjecture is hampered by the level of complexity of the theory of four-wave mixing for recoil induced resonances (see, e.g., Ref. [20]). Also, the nature of the four-wave mixing process differs substantially from the probe absorption: the four wave mixing signal is, in general, calculated as $|\rho_{eg}(p,p')|^2$, where $\rho_{eg}(p,p')$ is an off-diagonal element of a momentum-dependent density matrix. Since $\rho_{eg}(p,p')=\rho_{eg}(p,p')_{\mathrm{RZR}}+\rho_{eg}(p,p')_{\mathrm{RIR}}$, the interference terms $\rho_{eg}(p,p')_{\mathrm{RZR}}\times\rho_{ge}(p',p)_{\mathrm{RIR}}$ play an important role in the four-wave mixing signal. These terms are likely to be responsible for significant differences between four-wave mixing signals for the two circular probe polarizations. The theoretical work by Guo *et al.* [20] presents a derivation of the four-wave mixing resonances due to atomic recoil in a two-level system. However, for this theory to be applicable to our case, it should be complemented with the RZR contribution for systems with nonzero angular momenta.

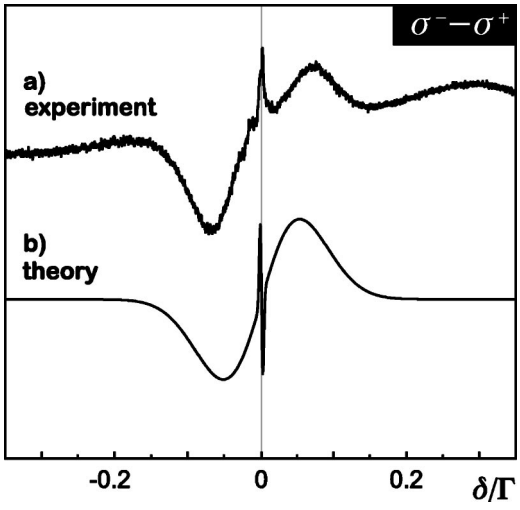

FIG. 8. The difference $\sigma^- - \sigma^+$ for the experimental absorption spectra presented in Fig. 7(a) compared with theoretical prediction (b).

E. Optical anisotropy of cold atoms

In Sec. IV A we discussed the RZR contribution to the MOT absorption spectra. It does not depend on the probe beam polarization, due to the fact that in the considered case of π-polarized pump field, neither populations of individual Zeeman sublevels, nor the Raman-resonance frequencies, depend on the sign of m_g. On the other hand, in the case of RIR, the polarization of the probe beam plays a crucial role. As was mentioned in the conclusions of Sec. IV B, recoil processes for two opposite circular polarizations of the probe result in dramatically different momentum and energy transfers. The momentum transfer from trapping beams perpendicular to the probe is the same for both probe beam polarizations and, according to Eq. (3), equals $\Delta p=\pm\hbar k\sqrt{2}/2$. However, the probe beam polarization selects which of the two pump beams, the co-propagating or the counterpropagating with the probe, is involved in the RIR. The quantity of the momentum transfer is $\Delta p\approx\pm\hbar k\theta$ for the σ^-- and $\Delta p\approx\pm 2\hbar k$ for the σ^+-polarized probe. Hence the RIR contribution is the cause of the obvious difference between the absorption spectra for the two probe beam polarizations around $\delta\approx 0$. Figure 8(a) exemplifies such a difference, obtained by subtraction of two independently measured absorption signals, compared with the calculated one [Fig. 8(b)]. While wide structures of the two curves (between $-0.1\,\Gamma$ and $+0.1\,\Gamma$) are well correlated, the agreement of their central parts is less satisfactory. The exact cause of this discrepancy

is not yet well understood. There are several possible effects that can influence that challenging recording of kHz-wide spectral features. On one hand, the accuracy with which we determine the zero of the pump-probe detuning is limited, the relative phase of the two laser beams undergoes some residual fluctuations, and the MOT parameters may vary between successive acquisitions of the σ^- and σ^+ spectra. On the other hand, additionally to the RZR and RIR contributions that we consider, the central structure might be systematically affected by additional mechanism such as, e.g., the Rayleigh scattering [1] or Faraday rotation due to imperfect compensation of a magnetic field and/or imperfect balancing of the MOT beams.

The asymmetry between absorption spectra, i.e., between optical properties of the sample as seen by probe beams of different polarizations, is known as *dichroism*, or generally as *optical anisotropy*. In our case, the atomic sample is placed in a center of a MOT, where $B=0$, and the optical pumping by pump beams creates atomic alignment, rather than polarization. Thus the optical anisotropy of our cold sample can be associated exclusively with the recoil processes. Consequently, when two absorption spectra for the σ^- and σ^+ probe beams are subtracted, the RZR contribution is completely eliminated and one is left only with the contribution from RIR's for the pump beams co- and counterpropagating with the probe.

The optical anisotropy associated with RIR and shown above (Fig. 8) constitutes experimental evidence of the effect recently predicted by Dubetsky and Berman [30]. The authors of Ref. [30] concentrated on the somewhat different experimental situation in which the optical anisotropy is detected via rotation of the polarization plane of a weak, linearly polarized probe beam propagating perpendicularly to the pump beam [31]. Still, the anisotropy described here has the same physical origin, the RIR.

V. CONCLUSIONS

We have successfully explained absorption spectra recorded in a working MOT. We have shown that full agreement between the theory and experimental data is attainable only when realistic MOT conditions, the light modulation in a trap and the quadrupole MOT magnetic field are taken into account. Our theoretical analysis emphasizes the importance of the atomic recoil processes in a MOT. Recoil-induced resonances have already been used in atomic velocimetry [13,14]. In order to apply this method to atoms in a working MOT, one has to eliminate other processes influencing the spectra, namely the Raman transitions between light-shifted Zeeman sublevels of the ground atomic state, RZR. For the MOT velocimetry based on RIR's, the RZR contribution appears as an undesired background which hinders precise determination of the RIR width. Unlike the RIR contribution, that due to the RZR is subject to significant inhomogeneous broadening by trap magnetic and light fields, so it is worthwhile to eliminate this background, e.g., such as suggested above by recording the optical anisotropy or the differential σ^+/σ^- absorption.

Let us note that in contrast to the experiment by Schadwinkel *et al.* [10] with carefully phase-stabilized trap beams, we see no contribution from the Raman transitions between vibrational levels associated with a possible optical lattice, whose frequencies could be in the similar range of the order of 100 kHz. We have found that under regular conditions in a standard MOT with nonstabilized trap beams, the short-term, random fluctuations of the trapping beam phases caused by mechanical instabilities of the setup, wash out the interference pattern, thus preventing stationary modulation of optical potential and atomic localization.

Another aspect of our results is the four-wave mixing spectroscopy. Since the four-wave mixing signals are generated in a more complex process, especially when the multilevel structure and recoil effects have to be taken into account, their theoretical analysis is complicated and requires further investigation. At the same time they appear to be far more sensitive to recoil processes than absorption, as the ultranarrow structures are here highly pronounced. This interesting feature motivates one to work out the method of MOT diagnostics based on four-wave mixing.

ACKNOWLEDGMENTS

This work was supported by the KBN (Grant No. 2P03B 088 26) and is part of a general program on cold-atom physics of the National Laboratory of AMO Physics in Torun, Poland. We are grateful to T. Pałasz for his contribution to the early stages of the experiment; A. Gabris for his help in numerical calculations; M. Trippenbach and D. Budker for stimulating discussions; and to D. Kimball, Sz. Pustelny, and S. Rochester for their comments on the manuscript.

[1] B. Lounis, J. Courtois, P. Verkerk, C. Salomon, and G. Grynberg, Phys. Rev. Lett. **69**, 3029 (1992).
[2] D. Grison, B. Lounis, C. Salomon, J. Y. Courtois, and G. Grynberg, Europhys. Lett. **15**, 149 (1991).
[3] See, for example, G. Grynberg and C. Robilliard, Phys. Rep. **355**, 335 (2001), and references therein.
[4] G. Grynberg, J.-Y. Courtois, B. Lounis, and P. Verkerk, Phys. Rev. Lett. **72**, 3017 (1994).
[5] P. Verkerk, B. Lounis, C. Salomon, C. Cohen-Tannoudji, and J. Courtois, Phys. Rev. Lett. **68**, 3861 (1992).
[6] Y.-C. Chen, Y.-W. Chen, J.-J. Su, J.-Y. Huang, and I. A. Yu, Phys. Rev. A **63**, 043808 (2001).
[7] G. C. Cardoso and J. W. R. Tabosa, Opt. Commun. **185**, 353 (2000).
[8] A. Hemmerich, M. Weidemüller, T. Esslinger, and T. W. Hänsch, Europhys. Lett. **21**, 445 (1993).
[9] J. W. R. Tabosa, G. Chen, Z. Hu, R. B. Lee, and H. J. Kimble, Phys. Rev. Lett. **66**, 3245 (1991).
[10] H. Schadwinkel, U. Reiter, V. Gomer, and D. Meschede, Phys. Rev. A **61**, 013409 (1999).

[11] A. Lezama, G. C. Cardoso, and J. W. R. Tabosa, Phys. Rev. A **63**, 013805 (2001).
[12] J. Zachorowski, T. Brzozowski, T. Pałasz, M. Zawada, and W. Gawlik, Acta Phys. Pol. A **101**, 61 (2002).
[13] D. R. Meacher, D. Boiron, H. Metcalf, C. Salomon, and G. Grynberg, Phys. Rev. A **50**, R1992 (1994).
[14] G. Di Domenico, G. Mileti, and P. Thomann, Phys. Rev. A **64**, 043408 (2001).
[15] M. C. Fischer, A. M. Dudarev, B. Gutiérrez-Medina, and M. G. Raizen, J. Opt. B: Quantum Semiclassical Opt. **3**, 279 (2001).
[16] E. L. Raab, M. Prentiss, A. Cable, S. Chu, and D. E. Pritchard, Phys. Rev. Lett. **59**, 2631 (1987).
[17] R. W. Boyd, *Nonlinear Optics* (Academic Press, New York, 1992).
[18] J.-Y. Courtois and G. Grynberg, Phys. Rev. A **48**, 1378 (1993).
[19] P. Verkerk, in Proceedings of The International School of Physics "Enrico Fermi," Course CXXXI, Varenna, 1996, edited by A. Aspect, W. Barretta, and R. Bonifacio (IOS Press, Amsterdam, 1996), p. 325.
[20] J. Guo, P. R. Berman, B. Dubetsky, and G. Grynberg, Phys. Rev. A **46**, 1426 (1992).
[21] J. Zachorowski, T. Pałasz, and W. Gawlik, Opt. Appl. **28**, 239 (1998).
[22] G. Wąsik, W. Gawlik, J. Zachorowski, and W. Zawadzki, Appl. Phys. B: Lasers Opt. **75**, 613 (2002).
[23] T. M. Brzozowski, M. Mączyńska, M. Zawada, J. Zachorowski, and W. Gawlik, J. Opt. B: Quantum Semiclassical Opt. **4**, 62 (2002).
[24] J.-Y. Courtois and G. Grynberg, Phys. Rev. A **46**, 7060 (1992).
[25] S. A. Hopkins and A. V. Durrant, Phys. Rev. A **56**, 4012 (1997).
[26] In our model, we consider the characteristic $\pi-\sigma^{\pm}$ pump-probe polarization configuration, which is the simplest one that can reproduce the shape of the observed spectra.
[27] J. H. Marquardt, H. G. Robinson, and L. Hollberg, J. Opt. Soc. Am. B **13**, 1384 (1996).
[28] J. Guo and P. R. Berman, Phys. Rev. A **47**, 4128 (1993).
[29] A. Lipsich, S. Barreiro, A. M. Akulshin, and A. Lezama, Phys. Rev. A **61**, 053803 (2000).
[30] B. Dubetsky and P. R. Berman, Phys. Rev. A **52**, R2519 (1995).
[31] In Ref. [30], the term Faraday rotation is used for the predicted rotation associated with RIR, though it is not due to any magnetic field. Some authors distinguish the magnetic-field from otherwise induced rotations by using the notions of "paramagnetic" and "diamagnetic" Faraday effects [32]. Similarly as in the recent review [33], we reserve the notion of the Faraday effect for a specific narrow class of effects exclusively related to the presence of the magnetic field and prefer to use the term optical anisotropy for the broad class of cases where the rotation is not related to the magnetic field, as in the case discussed in this paper.
[32] C. Cohen-Tannoudji and F. Laloë, J. Phys. (Paris) **28**, 505, (1967); **28**, 722 (1967).
[33] D. Budker, W. Gawlik, D. F. Kimball, S. M. Rochester, A. Weis, and V. V. Yashchuk, Rev. Mod. Phys. **74**, 1153 (2002).